

Searching for cosmic string induced stochastic gravitational wave background with the Parkes Pulsar Timing Array

Ligong Bian,^{1,2,*} Jing Shu,^{3,2,4,5,6,7,†} Bo Wang,⁷ Qiang Yuan,^{8,9,‡} and Junchao Zong^{10,4}

¹*Department of Physics and Chongqing Key Laboratory for Strongly Coupled Physics, Chongqing University, Chongqing 401331, China*

²*Center for High Energy Physics, Peking University, Beijing 100871, China*

³*School of Physics and State Key Laboratory of Nuclear Physics and Technology, Peking University, Beijing 100871, China*

⁴*CAS Key Laboratory of Theoretical Physics, Institute of Theoretical Physics, Chinese Academy of Sciences, Beijing 100190, China*

⁵*School of Physical Sciences, University of Chinese Academy of Sciences, Beijing 100049, China*

⁶*School of Fundamental Physics and Mathematical Sciences, Hangzhou Institute for Advanced Study, University of Chinese Academy of Sciences, Hangzhou 310024, China*

⁷*International Centre for Theoretical Physics Asia-Pacific,*

University of Chinese Academy of Sciences, 100190 Beijing, China

⁸*Key Laboratory of Dark Matter and Space Astronomy,*

Purple Mountain Observatory, Chinese Academy of Sciences, Nanjing 210023, China

⁹*School of Astronomy and Space Science, University of Science and Technology of China, Hefei 230026, China*

¹⁰*Department of Physics, Nanjing University, Nanjing 210093, China*

We search for stochastic gravitational wave background emitted from cosmic strings using the Parkes Pulsar Timing Array data over 15 years. While we find that the common power-law excess revealed by several pulsar timing array experiments might be accounted for by the gravitational wave background from cosmic strings, the lack of the characteristic Hellings-Downs correlation cannot establish its physical origin yet. The constraints on the cosmic string model parameters are thus derived with conservative assumption that the common power-law excess is due to unknown background. Two representative cosmic string models with different loop distribution functions are considered. We obtain constraints on the dimensionless string tension parameter $G\mu < 10^{-11} \sim 10^{-10}$, which is more stringent by two orders of magnitude than that obtained by the high-frequency LIGO-Virgo experiment for one model, and less stringent for the other. The results provide the chance to test the Grand unified theories, with the spontaneous symmetry breaking scale of $U(1)$ being two-to-three orders of magnitude below 10^{16} GeV. The pulsar timing array experiments are thus quite complementary to the LIGO-Virgo experiment in probing the cosmic strings and the underlying beyond standard model physics in the early Universe.

PACS numbers:

I. INTRODUCTION

Cosmic strings (CS) are one-dimensional topological defects supposed to be formed during phase transitions where symmetry gets broken spontaneously [1, 2]. The CS dynamics can be described by the Nambu-Goto action for thin and local strings with no internal structures. In this situation, infinite strings can reach the scaling regime [3–5] and go to loops through the intercommutation of intersecting string segments [6]. The formed small loops will oscillate and emit gravitational wave (GW) bursts by the structures of Cusps and Kinks [7, 8]. The superposition of uncorrelated GW bursts from many CSs form a stochastic gravitational wave background (SGWB). In the Nambu-Goto string scenario, the SGWB is characterized by the loop number density and the string tension (μ) [9]. The dimensionless parameter $G\mu$ (G is the Newtonian constant) that parameterized the gravitational interactions of strings is usually adopted in literature, which is tightly connect with the GUT scale ($M_{\text{GUT}} \sim 10^{16}$ GeV) as $G\mu \sim (\eta/M_{\text{GUT}})^2$ since CSs are generally predicted in the

symmetry breaking chain of grand unified theories (GUT). Therefore, the detection of SGWB from CSs provide an intriguing way to access the beyond-standard-model physics close to the GUT scale that are inaccessible by high-energy colliders [10–13], such as leptogenesis and the type-I seesaw scale [14].

The gravitational waves spectra from CSs span in a wide frequency range characterized by a plateau in the high-frequency region. The SGWB from CSs is one of the most promising target of LIGO-Virgo [15, 16], Laser Interferometer Space Antenna (LISA) [17], and pulsar timing arrays (PTA) [18, 19]. Recently, both LIGO-Virgo and PTA experiments made great progresses on the search of GWs. The LIGO-Virgo group place stringent constraints on the GW bursts and the SGWB from CSs in the high-frequency window [15]. In the nanohertz range, several PTAs reported the detection of a mysterious common red process [20–23], which may be explained as SGWB from various sources including CSs [24–27]. However, the GW interpretation of the common red process is still suspicious due to the lack of the characteristic Hellings-Downs (HD) correlation in the data. In this Letter we search for SGWB signals generated from CSs utilizing the Parkes Pulsar Timing Array (PPTA) data. We consider two representative SGWB models of CSs with two different loop distribution functions, and derive the constraints on the dimensionless $G\mu$ parameter of CS. The results can be

*Electronic address: lgybcl@cqu.edu.cn

†Electronic address: jshu@pku.edu.cn

‡Electronic address: yuanq@pmo.ac.cn

translated to constraints on the spontaneous symmetry breaking scale of the GUT.

II. SGWB SPECTRA FOR COSMIC STRING NETWORKS

The SGWB from cosmic string networks comes from the uncorrelated superpositions of GW bursts of three contributions: cusps, kinks, and kink-kink collision. The SGWB spectrum emitted from cosmic strings is given by

$$\Omega_{\text{GW}}(t_0, f) = \frac{f}{\rho_c} \frac{d\rho_{\text{GW}}}{df}(t_0, f), \quad (1)$$

where $\rho_c = \frac{3H_0^2}{8\pi G}$ is the critical energy density of the universe, $\frac{d\rho_{\text{GW}}}{df}(t_0, f)$ is the GWs energy density per unit frequency today. Considering different modes of loops oscillation (n), we have

$$\frac{d\rho_{\text{GW}}}{df}(t_0, f) = G\mu^2 \sum_n C_n(f) P_n, \quad (2)$$

where the $C_n(f)$ is a function of loop distributions depending on the cosmological background. To account for all contributions from cusps, kinks, and kink-kink collisions, we adopt the P_n from numerical simulations [28]. Analytically, $P_n = \frac{\Gamma}{\zeta(q)} n^{-q}$, $\Gamma \approx 50$ and $\zeta(q)$ is the Riemann zeta function with $q = 4/3, 5/3$, and 2 representing for cusps, kinks, and kink-kink collisions, respectively.

We first consider the SGWB from CSs with the loop production functions for non-self-intersecting loops being obtained directly from CS networks simulation in radiation and matter dominated era¹ by Blanco-Pillado, Olum, Shlaer [30, 31] (hereafter denoted as BOS model, which is dubbed as model A by LIGO-Virgo group in Ref. [15]). In the model, one need to take into account contributions from the radiation dominated era and the matter dominated era with the loop number density $n(l, t)$ given in the Supplemental Material. For the SGWB contributions from the radiation era, one has

$$C_n(f) = \frac{2n}{f^2} \int_{z_{\text{eq}}}^{z_{\text{cut}}} \frac{dz}{H_0 \sqrt{\Omega_r}(1+z)^8} n_r(l, t), \quad (3)$$

where z_{eq} is the redshift in the radiation-matter equality and z_{cut} is the cutoff redshift. The subscript r here denotes radiation dominated era, similarly, in the following rm is for the case where loops are formed in radiation dominated era but survive past to matter dominated era and m for the case of matter dominated era. We note that here the $n_r(l, t)$ is the loop distribution function rather than the oscillation mode n before the integration. The SGWB contributions from matter dominated era constitute two parts: loops that survive to matter

dominated era and loops formed in matter dominated era. The C_n takes the form of

$$C_n(f) = \frac{2n}{f^2} \int_0^{z_{\text{eq}}} \frac{dz}{H_0 \sqrt{\Omega_m}(1+z)^{15/2}} n_i(l, t), \quad (4)$$

with i being rm and m for these two cases, respectively.

Following the same procedure, we can calculate the SGWB spectrum with loop distribution functions being derived analytically by Lorenz, Ringeval, and Sakellariadou [32] (denoted as LRS, which is dubbed as model B by LIGO-Virgo group in Ref. [15]), where the distribution of non-self-intersecting scaling loops are extracted from simulations [33]. In the model, the contribution from the radiation dominated era takes the form of

$$\Omega_{\text{GW}}(f) = \frac{64\pi G^2 \mu^2 \Omega_r}{3} \sum_n P_n \int dx n(x), \quad (5)$$

and in the matter dominated era, the GW spectrum is

$$\Omega_{\text{GW}}(f) = \frac{162\pi G^2 \mu^2}{\Omega_m^{-2} H_0^{-2}} \frac{1}{f^2} \sum_n P_n n^2 \int dx n(x). \quad (6)$$

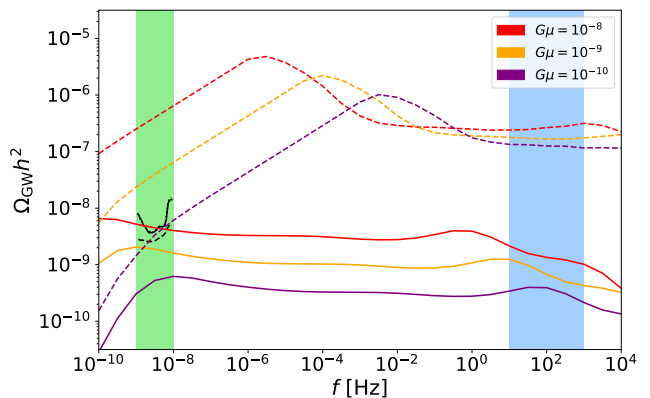


FIG. 1: Expected spectra of SGWB from CS for the BOS (LRS) model with $G\mu = 10^{-8}, 10^{-9}$, and 10^{-10} , which are indicated by red, orange and purple solid (dashed) lines. The solid and dashed black lines represent the 95% C.L. upper limits for free spectrum assumption derived from the PPTA data for different hypotheses (H2/H3 and H4 in Tables I and II, respectively). The sensitive frequency regions of PTA and LIGO-Virgo are denoted by green and blue shaded bands.

Fig. 1 shows the total SGWB spectra of the CS-induced SGWB for the BOS and LRS models, for a few values of $G\mu$. It is shown that the BOS model predicts relatively flat spectra (solid lines) and hence the PTA experiment is more suitable to probe it. On the other hand, the LRS model predicts harder spectra (dashed lines) which is more optimal for the high-frequency GW experiment such as LIGO-Virgo. Also shown in Fig. 1 are the upper limits of the free-spectrum SGWB derived from the PPTA data [34]. We find that the CS models with $G\mu$ of $10^{-8} \sim 10^{-10}$ are severely constrained by the PPTA data. The magnitude of the SGWB spectra for the LRS model is much higher than that of the BOS model at high frequencies due to more small loops in the loop distribution function dominate in such frequency range.

¹ It was noted that the inflation might also dilute the CS networks if CSs were formed before the onset of the inflation, in which case the nano-hertz GW experiments may not be sensitive to probe the SGWB from CSs [29].

III. DATA ANALYSIS

The dataset we used in this work is the second data release (DR2) of the PPTA [35], which is available in the CSIRO pulsar data archive². Searches for SGWBs and other fundamental physics problems using these data (or the subsets) were also carried out [21, 34, 36–38]. In PTA, to search for such an SGWB signal from CS is to find spatially correlated time residuals among time-of-arrivals (ToA) of different pulsars. The residuals are composed of deterministic timing models, noises, and the hypothetical signal (SGWB from CS here). We use the TEMPO2 tool [39, 40] to fit the timing models of pulsars, the ENTERPRISE³ and the ENTERPRISE_EXTENSIONS⁴ to model the noises, and PTMCMCSampler [41] to do the Bayesian analysis. The noise model is based on single pulsar analyses of Ref. [42]. Briefly speaking, the stochastic noises mainly include two parts, the white noise and red noise. The white noise may come from the radio frequency interference, pulse profile changes or instrumental artifacts. We use three parameters, EFAC (Error FACtor), EQUAD (Error added in QUADrature) and ECORR (Error of CORRelation between ToAs in a single epoch), to account for white noise which can not be subtracted by fitting the timing model. As usually done [37, 38], we fix the white noise parameters as their maximum likelihood values from the single pulsar analyses in the Bayesian analysis. The red noises are mainly caused by the irregularities of the pulsar spin (spin noise) and the dispersion measure of photons when traveling through the interstellar medium (DM noise). For some pulsars there are band noise for ToAs of a certain photon frequency band and chromatic noise which correlates between different photon frequencies. All the red noises are modeled as power-law forms with amplitude A and slope γ . Several analyses revealed that there is a common power-law (CPL) process in the pulsar ToAs, whose nature is still in debate [20–23]. In this work we will test different assumptions on the CPL, as either the SGWB signal from CS (see also [24, 25]) or an unknown background. The solar system ephemeris uncertainties are modeled with a 11-parameter model `BayesEphem` implemented in ENTERPRISE, including perturbations in masses of major planets, the drift rate of the Earth-Moon barycenter orbit, and the perturbations of the Earth’s orbit from Jupiter’s average orbital elements described by 6 parameters [43]. We summarize the noise and signal parameters together with their priors adopted in the Bayesian analysis in Table S1 in the Supplemental Material.

IV. RESULT

To address how significant the CS-induced SGWB signals in the data, we test the Bayes factor (BF) of the “signal hy-

pothesis” against the null hypothesis, following the Savage-Dickey formula [44]

$$\text{BF}_{10} = \frac{P_1(\mathbf{D})}{P_0(\mathbf{D})} = \frac{P(\boldsymbol{\phi} = \boldsymbol{\phi}_0)}{P(\boldsymbol{\phi} = \boldsymbol{\phi}_0|\mathbf{D})}, \quad (7)$$

where BF_{10} means the BF of hypothesis H1 against H0, \mathbf{D} is the observational data, $\boldsymbol{\phi}$ is the parameters of the signal model, and $\boldsymbol{\phi}_0$ is the parameters of the null hypothesis which is a subset of $\boldsymbol{\phi}$. P_0 and P_1 are the evidence of the noise and signal hypotheses. The BF_{10} is equivalent to the ratio of the prior to the posterior probabilities of the null hypothesis.

The null hypothesis (H0) corresponds to the model with only the pulsar timing model and noise. For hypothesis H1, we assume an additional CPL process in the model. The CS model with the HD correlation is included in substitution of the CPL process is labelled as H2. In addition, in H3 and H4 we consider simultaneously the CPL process as an unknown systematics and the CS contribution, in which the auto-correlation of a pulsar’s own ToAs is not subtracted (H3) and subtracted (H4), respectively. The results of the fittings for different hypotheses are summarized in Tables I and II.

For hypothesis H1, a clear CPL signal with a BF of $10^{3.2}$ is revealed in the data, consistent with previous studies [20–23]. The posterior distributions of the CPL model parameters are shown in Fig. S1 in the Supplemental Material. Similar signal with comparable BF value is found if we assume a CS-induced SGWB component in the model rather than the CPL (H2). Fitting results of the CS parameter $\log_{10} G\mu$ are -10.38 ± 0.21 and $-10.89_{-0.17}^{+0.14}$ for the BOS and LRS model, with 1σ error bars presented. The corresponding parameter values are consistent with that employed to account for the NANOGrav data, but with different model assumptions [24]. Since the nature of the CPL process is unclear, and particularly the characteristic HD correlation of GWs is still lack, we also test the hypotheses that treating the CPL as an unknown background. The resulting BF of hypotheses H3 or H4 against H1 is close to 1 which means that the evidence of the CS is not significant in case of a CPL background. We therefore derive the 95% credible level (C.L.) upper limits on $\log_{10} G\mu$, as given in Tables I and II. The posterior distributions of the CPL and CS parameters for H4 are shown in Fig. 2. More results of the analysis based on different hypotheses can be found in Figs. S2-S3 in the Supplemental Material. Additional tests assuming that the CPL has an astrophysical origin from the supermassive binary black hole (SMBBH) give similar conclusion (see the Supplemental Material).

Our results can be compared with those obtained by the LIGO-Virgo observations of high-frequency GWs [15], which is displayed in Fig. 3. We also show the bound from the cosmic microwave background (CMB), while the less stronger limit from Big Bang nucleosynthesis (BBN) is too weak to be shown in the figure [15, 45]. The LIGO-Virgo upper limits of $G\mu$ are $10^{-8} - 10^{-6}$ and $(4.0 - 6.3) \times 10^{-15}$ for the BOS and LRS model (model A and B in [15]), respectively. Compared with LIGO-Virgo results, the PPTA upper limits on $\log_{10} G\mu$ improve by more than two orders of magnitude for the BOS model. For the LRS model, the LIGO-Virgo result is more stringent because the SGWB spectrum is harder. The PTA ex-

² <https://doi.org/10.4225/08/5aff8174e9b3>

³ <https://github.com/nanograv/enterprise>

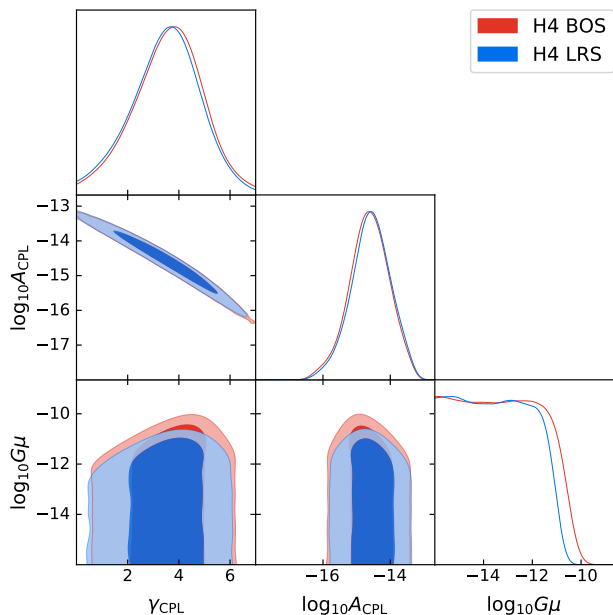
⁴ <https://github.com/nanograv/enterprise.extensions>

TABLE I: Hypotheses, Bayes factors, and estimated model parameters for the BOS model.

Hypothesis	Pulsar Noise	CPL Process	HD process CS spectrum	Bayes Factors	Parameter Estimation (1σ interval)	
					$\log_{10} G\mu$	$\log_{10} A_{\text{CPL}}, \gamma_{\text{CPL}}$
H0:Pulsar Noise	✓					
H1:CPL	✓	✓		$10^{3.2}$ (/H0)		$-14.48^{+0.62}_{-0.64}, 3.34^{+1.37}_{-1.53}$
H2:CS	✓		✓(full HD)	$10^{3.1}$ (/H0)	$-10.38^{+0.21}_{-0.21}$	
H3:CS1	✓	✓	✓(full HD)	1.96 (/H1)	< -10.02 (95% C.L.)	$-15.58^{+1.21}_{-1.64}, 3.11^{+1.95}_{-2.02}$
H4:CS2	✓	✓	✓(no-auto HD)	0.60 (/H1)	< -10.54 (95% C.L.)	$-14.61^{+0.58}_{-0.59}, 3.63^{+1.24}_{-1.40}$

TABLE II: Hypotheses, Bayes factors, and estimated model parameters for the LRS model.

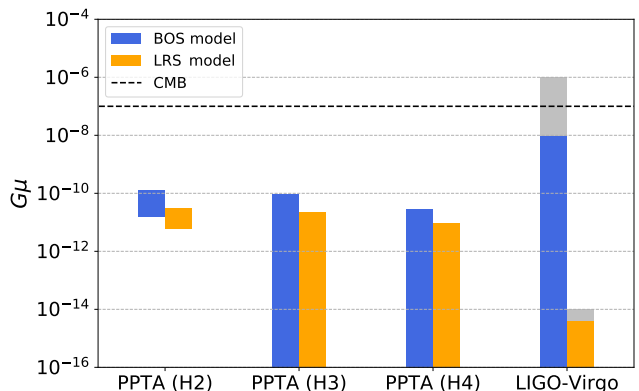
Hypothesis	Pulsar Noise	CPL process	HD process CS spectrum	Bayes Factors	Parameter Estimation (1σ interval)	
					$\log_{10} G\mu$	$\log_{10} A_{\text{CPL}}, \gamma_{\text{CPL}}$
H0:Pulsar Noise	✓					
H1:CPL	✓	✓		$10^{3.2}$ (/H0)		$-14.48^{+0.62}_{-0.64}, 3.34^{+1.37}_{-1.53}$
H2:CS	✓		✓(full HD)	$10^{3.3}$ (/H0)	$-10.89^{+0.14}_{-0.17}$	
H3:CS1	✓	✓	✓(full HD)	1.62 (/H1)	< -10.64 (95% C.L.)	$-15.44^{+1.18}_{-1.74}, 3.08^{+1.94}_{-1.99}$
H4:CS2	✓	✓	✓(no-auto HD)	0.55 (/H1)	< -11.04 (95% C.L.)	$-14.57^{+0.58}_{-0.59}, 3.54^{+1.24}_{-1.41}$

FIG. 2: Posteriors distribution of $\log_{10} G\mu$ and the CPL parameters of BOS (red) and LRS (blue) models assuming a no-auto HD correlation. The 1σ and 2σ regions are presented in light and dark colors.

periment is thus very complementary to the LIGO-Virgo experiment for the searches of CS-induced SGWB.

V. CONCLUSION

The very precise timing measurements of pulsars provide a powerful tool to probe the fundamental new physics process occurred in the early Universe. In this work we use more

FIG. 3: Constraints on $G\mu$ at the 95% C.L. from the PPTA data for different hypotheses, compared with those obtained by LIGO-Virgo experiment [15]. Silver boxes represent the ranges reported in the LIGO-Virgo analysis. The limit from cosmic microwave background (CMB) is also reported by the black dashed line [45].

than 15 years of observations of 26 millisecond pulsars by the PPTA experiment to search for SGWB from CS networks. We show that the CPL process revealed by several PTAs recently can be explained by the CS-induced SGWB signal with $\log_{10} G\mu \sim -10.38$ and -10.89 for the two typical classes of CS models, the BOS and LRS models. While the LRS model explanation would be excluded by the LIGO-Virgo observations at high frequencies, the BOS model explanation is consistent with the LIGO-Virgo data [15]. As a conservative alternative, we also assume the CPL as a background component and turn to set limits on the CS model parameters. The PPTA upper limits on $\log_{10} G\mu$ reach about $-10 \sim -11$, depending on the CS models and the analysis methods. These constraints correspond to the symmetry breaking scale $\eta \sim 10^{13} - 10^{14}$ GeV, that challenge the grand unification theories below the

GUT scale already. For the BOS model, the PPTA limits are more stringent than those from LIGO-Virgo, and for the LRS model the LIGO-Virgo experiment is more sensitive. This is due to the fact that, in the LRS model, more small loops are contained in the loop distribution functions that control the behaviours of the SGWB spectra from CS networks in high frequency range. We expect that continuous accumulation of more precise data by PTAs around the world in the near future will critically test the CS models and more generally, a class of GUTs admitting the $U(1)$ symmetry breaking in the early Universe.

VI. ACKNOWLEDGEMENTS

This work uses the public data from the Parkes Pulsar Timing Array. We thank Huai-Ke Guo and Yue Zhao for useful discussions, and appreciate Xiao Xue for the help on the

data analysis in the early stage of this work. L.B. is supported by the National Key Research and Development Program of China under Grant No. 2021YFC2203004, the National Natural Science Foundation of China (NSFC) under Grants No. 12075041 and No. 12047564, the Fundamental Research Funds for the Central Universities of China under Grants No. 2021CDJQY-011 and No. 2020CDJQY-Z003, and Chongqing Natural Science Foundation under Grant No. cstc2020jcyj-msxmX0814. J. S. is supported by the NSFC under Grants No. 12025507, No. 11690022, and No. 11947302, by the Strategic Priority Research Program and Key Research Program of Frontier Science of the Chinese Academy of Sciences (CAS) under Grants No. XDB21010200, No. XDB23010000, No. XDPB15, and No. ZDBS-LY-7003, and by the CAS Project for Young Scientists in Basic Research under Grant No. YSBR-006. Q.Y. is supported by the Program for Innovative Talents and Entrepreneur in Jiangsu and the Key Research Program of CAS under Grant No. XDPB15.

-
- [1] T. W. B. Kibble, “Topology of Cosmic Domains and Strings,” *J. Phys. A*, vol. 9, pp. 1387–1398, 1976.
- [2] M. B. Hindmarsh and T. W. B. Kibble, “Cosmic strings,” *Rept. Prog. Phys.*, vol. 58, pp. 477–562, 1995.
- [3] D. P. Bennett and F. R. Bouchet, “Evidence for a Scaling Solution in Cosmic String Evolution,” *Phys. Rev. Lett.*, vol. 60, p. 257, 1988.
- [4] B. Allen and E. P. S. Shellard, “Cosmic string evolution: a numerical simulation,” *Phys. Rev. Lett.*, vol. 64, pp. 119–122, 1990.
- [5] M. Sakellariadou and A. Vilenkin, “Cosmic-string evolution in flat space-time,” *Phys. Rev. D*, vol. 42, pp. 349–353, 1990.
- [6] T. Vachaspati and A. Vilenkin, “Formation and Evolution of Cosmic Strings,” *Phys. Rev. D*, vol. 30, p. 2036, 1984.
- [7] T. Damour and A. Vilenkin, “Gravitational wave bursts from cusps and kinks on cosmic strings,” *Phys. Rev. D*, vol. 64, p. 064008, 2001.
- [8] T. Damour and A. Vilenkin, “Gravitational wave bursts from cosmic strings,” *Phys. Rev. Lett.*, vol. 85, pp. 3761–3764, 2000.
- [9] A. Vilenkin and E. P. S. Shellard, *Cosmic Strings and Other Topological Defects*. Cambridge University Press, 7 2000.
- [10] S. F. King, S. Pascoli, J. Turner, and Y.-L. Zhou, “Confronting SO(10) GUTs with proton decay and gravitational waves,” *JHEP*, vol. 10, p. 225, 2021.
- [11] S. F. King, S. Pascoli, J. Turner, and Y.-L. Zhou, “Gravitational Waves and Proton Decay: Complementary Windows into Grand Unified Theories,” *Phys. Rev. Lett.*, vol. 126, no. 2, p. 021802, 2021.
- [12] W. Buchmuller, V. Domcke, H. Murayama, and K. Schmitz, “Probing the scale of grand unification with gravitational waves,” *Phys. Lett. B*, vol. 809, p. 135764, 2020.
- [13] R. Caldwell *et al.*, “Detection of Early-Universe Gravitational Wave Signatures and Fundamental Physics,” 3 2022.
- [14] J. A. Dror, T. Hiramatsu, K. Kohri, H. Murayama, and G. White, “Testing the Seesaw Mechanism and Leptogenesis with Gravitational Waves,” *Phys. Rev. Lett.*, vol. 124, no. 4, p. 041804, 2020.
- [15] R. Abbott *et al.*, “Constraints on Cosmic Strings Using Data from the Third Advanced LIGO–Virgo Observing Run,” *Phys. Rev. Lett.*, vol. 126, no. 24, p. 241102, 2021.
- [16] B. P. Abbott *et al.*, “Constraints on cosmic strings using data from the first Advanced LIGO observing run,” *Phys. Rev. D*, vol. 97, no. 10, p. 102002, 2018.
- [17] P. Auclair *et al.*, “Probing the gravitational wave background from cosmic strings with LISA,” *JCAP*, vol. 04, p. 034, 2020.
- [18] N. Yonemaru *et al.*, “Searching for gravitational wave bursts from cosmic string cusps with the Parkes Pulsar Timing Array,” *Mon. Not. Roy. Astron. Soc.*, vol. 501, no. 1, pp. 701–712, 2021.
- [19] S. A. Sanidas, R. A. Battye, and B. W. Stappers, “Constraints on cosmic string tension imposed by the limit on the stochastic gravitational wave background from the European Pulsar Timing Array,” *Phys. Rev. D*, vol. 85, p. 122003, 2012.
- [20] Z. Arzoumanian *et al.*, “The NANOGrav 12.5 yr Data Set: Search for an Isotropic Stochastic Gravitational-wave Background,” *Astrophys. J. Lett.*, vol. 905, no. 2, p. L34, 2020.
- [21] B. Goncharov *et al.*, “On the Evidence for a Common-spectrum Process in the Search for the Nanohertz Gravitational-wave Background with the Parkes Pulsar Timing Array,” *Astrophys. J. Lett.*, vol. 917, no. 2, p. L19, 2021.
- [22] S. Chen *et al.*, “Common-red-signal analysis with 24-yr high-precision timing of the European Pulsar Timing Array: inferences in the stochastic gravitational-wave background search,” *Mon. Not. Roy. Astron. Soc.*, vol. 508, no. 4, pp. 4970–4993, 2021.
- [23] J. Antoniadis *et al.*, “The International Pulsar Timing Array second data release: Search for an isotropic gravitational wave background,” *Mon. Not. Roy. Astron. Soc.*, vol. 510, no. 4, pp. 4873–4887, 2022.
- [24] J. Ellis and M. Lewicki, “Cosmic String Interpretation of NANOGrav Pulsar Timing Data,” *Phys. Rev. Lett.*, vol. 126, no. 4, p. 041304, 2021.
- [25] L. Bian, R.-G. Cai, J. Liu, X.-Y. Yang, and R. Zhou, “Evidence for different gravitational-wave sources in the NANOGrav dataset,” *Phys. Rev. D*, vol. 103, no. 8, p. L081301, 2021.
- [26] S. Blasi, V. Brdar, and K. Schmitz, “Has NANOGrav found first evidence for cosmic strings?,” *Phys. Rev. Lett.*, vol. 126, no. 4, p. 041305, 2021.
- [27] J. J. Blanco-Pillado, K. D. Olum, and J. M. Wachter, “Comparison of cosmic string and superstring models to NANOGrav 12.5-year results,” *Phys. Rev. D*, vol. 103, no. 10, p. 103512, 2021.

- 2021.
- [28] J. J. Blanco-Pillado and K. D. Olum, “Stochastic gravitational wave background from smoothed cosmic string loops,” *Phys. Rev. D*, vol. 96, no. 10, p. 104046, 2017.
 - [29] Y. Cui, M. Lewicki, and D. E. Morrissey, “Gravitational Wave Bursts as Harbingers of Cosmic Strings Diluted by Inflation,” *Phys. Rev. Lett.*, vol. 125, no. 21, p. 211302, 2020.
 - [30] J. J. Blanco-Pillado, K. D. Olum, and B. Shlaer, “The number of cosmic string loops,” *Phys. Rev. D*, vol. 89, no. 2, p. 023512, 2014.
 - [31] J. J. Blanco-Pillado, K. D. Olum, and B. Shlaer, “Large parallel cosmic string simulations: New results on loop production,” *Phys. Rev. D*, vol. 83, p. 083514, 2011.
 - [32] L. Lorenz, C. Ringeval, and M. Sakellariadou, “Cosmic string loop distribution on all length scales and at any redshift,” *JCAP*, vol. 10, p. 003, 2010.
 - [33] C. Ringeval, M. Sakellariadou, and F. Bouchet, “Cosmological evolution of cosmic string loops,” *JCAP*, vol. 02, p. 023, 2007.
 - [34] X. Xue *et al.*, “Constraining Cosmological Phase Transitions with the Parkes Pulsar Timing Array,” *Phys. Rev. Lett.*, vol. 127, no. 25, p. 251303, 2021.
 - [35] M. Kerr *et al.*, “The Parkes Pulsar Timing Array project: second data release,” *Publ. Astron. Soc. Austral.*, vol. 37, p. e020, 2020.
 - [36] R. M. Shannon *et al.*, “Gravitational waves from binary supermassive black holes missing in pulsar observations,” *Science*, vol. 349, no. 6255, pp. 1522–1525, 2015.
 - [37] N. K. Porayko *et al.*, “Parkes Pulsar Timing Array constraints on ultralight scalar-field dark matter,” *Phys. Rev. D*, vol. 98, no. 10, p. 102002, 2018.
 - [38] X. Xue *et al.*, “High-precision search for dark photon dark matter with the Parkes Pulsar Timing Array,” *Phys. Rev. Res.*, vol. 4, no. 1, p. L012022, 2022.
 - [39] G. Hobbs, R. Edwards, and R. Manchester, “Tempo2, a new pulsar timing package. 1. overview,” *Mon. Not. Roy. Astron. Soc.*, vol. 369, pp. 655–672, 2006.
 - [40] R. T. Edwards, G. B. Hobbs, and R. N. Manchester, “Tempo2, a new pulsar timing package. 2. The timing model and precision estimates,” *Mon. Not. Roy. Astron. Soc.*, vol. 372, pp. 1549–1574, 2006.
 - [41] J. Ellis and R. van Haasteren, “jellis18/ptmcmcsampler: Official release,” Oct. 2017.
 - [42] B. Goncharov *et al.*, “Identifying and mitigating noise sources in precision pulsar timing data sets,” *Mon. Not. Roy. Astron. Soc.*, vol. 502, no. 1, pp. 478–493, 2021.
 - [43] Z. Arzoumanian *et al.*, “The NANOGrav 11-year Data Set: Pulsar-timing Constraints On The Stochastic Gravitational-wave Background,” *Astrophys. J.*, vol. 859, no. 1, p. 47, 2018.
 - [44] J. M. Dickey, “The weighted likelihood ratio, linear hypotheses on normal location parameters,” *The Annals of Mathematical Statistics*, vol. 42, no. 1, pp. 204–223, 1971.
 - [45] P. A. R. Ade *et al.*, “Planck 2013 results. XXV. Searches for cosmic strings and other topological defects,” *Astron. Astrophys.*, vol. 571, p. A25, 2014.

Supplemental material

A. CS loop distributions

The BOS model. — In this model, the loop production functions are inferred from Nambu-Goto simulations of CS networks in radiation and matter dominated era directly. In the radiation dominated era, we take $l/t \leq 0.1$ to consider the cut-off of the maximum size of loops. In the matter dominated era, as suggested by simulations, plenty of loops formed in the radiation era will survive till the time of radiation-matter equality and emit GWs in the matter dominated era, which imposes a constrain on loop size, $l/t < 0.09t_{\text{eq}}/t - \Gamma G\mu$. Furthermore, loops can also be produced when the CS networks reach the scaling regime in the matter dominated era, in which case the loop size should satisfy $l/t < 0.18$. The loop distribution functions of all the circumstances are

$$n_r(l, t) = \frac{0.18}{t^{3/2}(l + \Gamma G\mu t)^{5/2}}, l/t \leq 0.1, \quad (\text{S1})$$

$$n_{rm}(l, t) = \frac{0.18t_{\text{eq}}^{1/2}}{t^2(l + \Gamma G\mu t)^{5/2}}, l/t < 0.09t_{\text{eq}}/t - \Gamma G\mu, \quad (\text{S2})$$

$$n_m(l, t) = \frac{0.27 - 0.45(l/t)^{0.31}}{t^2(l + \Gamma G\mu t)^2}, l/t < 0.18. \quad (\text{S3})$$

The LRS model. — Different from the BOS model, in the LRS model, the loop distribution of the non-self-intersecting scaling loops rather than the loop production function is inferred from CS network simulations [32]. On scales $x = l/t \gg \Gamma G\mu \equiv x_d$, the simulation gives

$$n(x) = \frac{C_0}{x^p}, \quad (\text{S4})$$

where the two constants C_0 and p in the radiation dominated era and matter dominated era are

$$p = 0.60^{+0.21}_{-0.15}|_r, \quad p = 0.41^{+0.08}_{-0.07}|_m, \quad (\text{S5})$$

$$C_0 = 0.21^{+0.12}_{-0.13}|_r, \quad C_0 = 0.09^{+0.03}_{-0.03}|_m. \quad (\text{S6})$$

Note that, not only loops would emit GWs — which decreases their length l — but the GW emission also back-reacts on the loops. The back-reaction smooths out the loops on the smallest scales (in particular the kinks), hindering the formation of smaller loops. To extend the loop distribution given above down to smaller scales, a further length scale $x_c \ll x_d$ (the so-called “gravitational back-reaction scale”) is introduced, which is estimated as $x_c = 20(G\mu)^{1+2\chi}$ through matching the loop distribution on scales $x \gg x_d$ (Eq. (S4)), where $\chi_r = 0.2^{+0.07}_{-0.10}$ for the radiation dominated era and $\chi_m = 0.295^{+0.03}_{-0.04}$ for the matter dominated era [17]. The specific distributions in all periods are then given by [32]

$$n(x > x_d) \simeq \frac{C}{(x + x_d)^{3-2\chi}}, \quad (\text{S7})$$

$$n(x_c < x < x_d) \simeq \frac{C(3\nu - 2\chi - 1)}{2 - 2\chi} \frac{1}{x_d} \frac{1}{x^{2(1-\chi)}}, \quad (\text{S8})$$

$$n(x < x_c < x_d) \simeq \frac{C(3\nu - 2\chi - 1)}{2 - 2\chi} \frac{1}{x_c^{2(1-\chi)}} \frac{1}{x_d}, \quad (\text{S9})$$

where $C = C_0(1 - \nu)^{2-p}$, and $\nu = 1/2$ for radiation dominated era and $\nu = 2/3$ for matter dominated era.

B. PTA model parameters

Table S1 summarizes the major model parameters and their prior distributions of the noise and signal components used in the analysis. The timing model parameters of each pulsar are not listed here.

C. Results of other Hypotheses

Fig. S1 shows the parameter distributions of the CPL process (H1). The best-fitting values and 1σ errors of the amplitude and spectral index are $\log_{10} A_{\text{CPL}} = -14.48^{+0.62}_{-0.64}$ and $\gamma_{\text{CPL}} = 3.34^{+1.37}_{-1.53}$. The BF of the hypothesis H1 against the null hypothesis H0 is $10^{3.2}$, indicating a strong evidence of the exist of such a component.

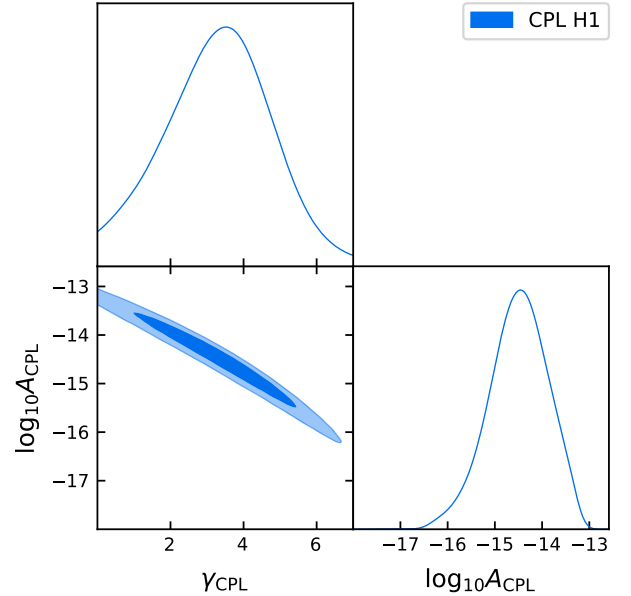


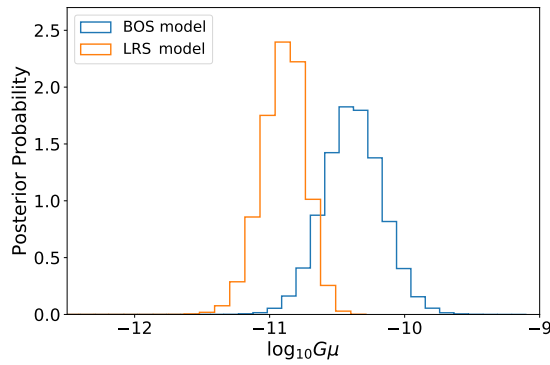
FIG. S1: Posterior distributions of the amplitude $\log_{10} A_{\text{CPL}}$ and power-law index γ_{CPL} of the CPL component for hypothesis H1.

Then we search for the signal of SGWB from the CS. Fig. S2 shows the one-dimensional probability distributions of the CS parameter $G\mu$ without including the CPL process (H2). This test reveals that the CS-induced SGWB can be used to explain the CPL excess in the data, with similar BFs compared with the CPL assumption.

Fig. S3 gives the posterior distributions of the CPL parameters and the CS parameter for hypothesis H3. In this case, the CS signal is not evident, and we can derive constraints on the CS parameter. At the 95% C.L., we find $\log_{10} G\mu < -10.02$ (-10.64) for the BOS (LRS) model. Similar analysis but re-

TABLE S1: Parameters and their prior distribution in data analysis. U and log-U stand for the uniform and log-uniform distribution.

parameter	Description	Prior	Comments
Noise parameters(θ)			
EFAC	White-noise modifier per backend	U [0, 10]	Fixed for setting limits
EQUAD	Quadratic white noise per backend	log-U [-10, -5]	Fixed for setting limits
ECORR	Correlated-ToAs white noise per backend	log-U [-10, -5]	Fixed for setting limits
A_{SN}	Spin-noise amplitude	log-U [-20, -6] (search) U [10^{-20} , 10^{-6}] (limit)	One parameter per pulsar
γ_{SN}	Spin-noise spectral index	U [0, 10]	One parameter per pulsar
A_{DM}	DM-noise amplitude	log-U [-20, -6] (search) U [10^{-20} , 10^{-6}] (limit)	One parameter per pulsar
γ_{DM}	DM-noise spectral index	U [0, 10]	One parameter per pulsar
A_{BAND}	Band-noise amplitude	log-U [-20, -6] (search) U [10^{-20} , 10^{-6}] (limit)	One parameter partial pulsars
γ_{BAND}	Band-noise spectral index	U [0, 10]	One parameter partial pulsars
A_{CHROM}	Chromatic-noise amplitude	log-U [-20, -6] (search) U [10^{-20} , 10^{-6}] (limit)	One parameter partial pulsars
γ_{CHROM}	Chromatic-noise spectral index	U [0, 10]	One parameter partial pulsars
n_{CHROM}	Index of chromatic effects	U [0, 6]	Fixed for single pulsar
A_{CPL}	CPL process amplitude	log-U [-18, -11] (search) U [10^{-18} , 10^{-11}] (limit)	One parameter per PTA
γ_{CPL}	CPL process power index	U [0, 7]	One parameter per PTA
Signal parameters (ψ)			
$G\mu$	String tension	log-U [-16, -7] (search) U [10^{-16} , 10^{-7}] (limit)	One parameter per PTA
BayesEphem parameters (ϕ)			
z_{drift}	Drift-rate of Earth's orbit about ecliptic z -axis	U[- 10^{-9} , 10^{-9}] rad yr $^{-1}$	One parameter per PTA
$\Delta M_{\text{Jupiter}}$	Perturbation of Jupiter's mass	$N(0, 1.5 \times 10^{-11}) M_{\odot}$	One parameter per PTA
ΔM_{Saturn}	Perturbation of Saturn's mass	$N(0, 8.2 \times 10^{-12}) M_{\odot}$	One parameter per PTA
ΔM_{Uranus}	Perturbation of Uranus' mass	$N(0, 5.7 \times 10^{-11}) M_{\odot}$	One parameter per PTA
$\Delta M_{\text{Neptune}}$	Perturbation of Neptune's mass	$N(0, 7.9 \times 10^{-11}) M_{\odot}$	One parameter per PTA
PCA_i	Principal components of Jupiter's orbit	U [-0.05, 0.05]	One parameter per PTA

FIG. S2: Posteriors distribution of $\log_{10} G\mu$ for hypothesis H2, for the BOS and LRS models.

moving the auto-correlation of the pulsars' ToAs (H4) is pre-

sented in the main text.

Finally we consider the possibility that the CPL has an astrophysical origin from the supermassive binary black holes (SMBBH). The spectrum of the SMBBH SGWB signal is given by

$$S(f) = \frac{A_{\text{SMBBH}}^2}{12\pi^2} \left(\frac{f}{\text{yr}^{-1}} \right)^{\gamma_{\text{SMBBH}}} \text{yr}^3, \quad (\text{S10})$$

where the power-law index γ_{SMBBH} is fixed to be 13/3. The prior of $\log_{10} A_{\text{SMBBH}}$ is assumed to be uniformly distributed in [-18, -14]. We test three model assumptions, with H5 being the SMBBH-only hypothesis and H6 (H7) being the SMBBH + CS for the BOS (LRS) model.

The constraints on the model parameters of hypotheses H5 - H7 are shown in Fig. S4, Fig. S5, and Table S2. The CPL process may also be explained by the SMBBH signal, with $\log_{10} A_{\text{SMBBH}} = -14.89^{+0.10}_{-0.12}$. For hypotheses H6 and H7, we reach similar conclusion with H3 or H4 where the CPL is

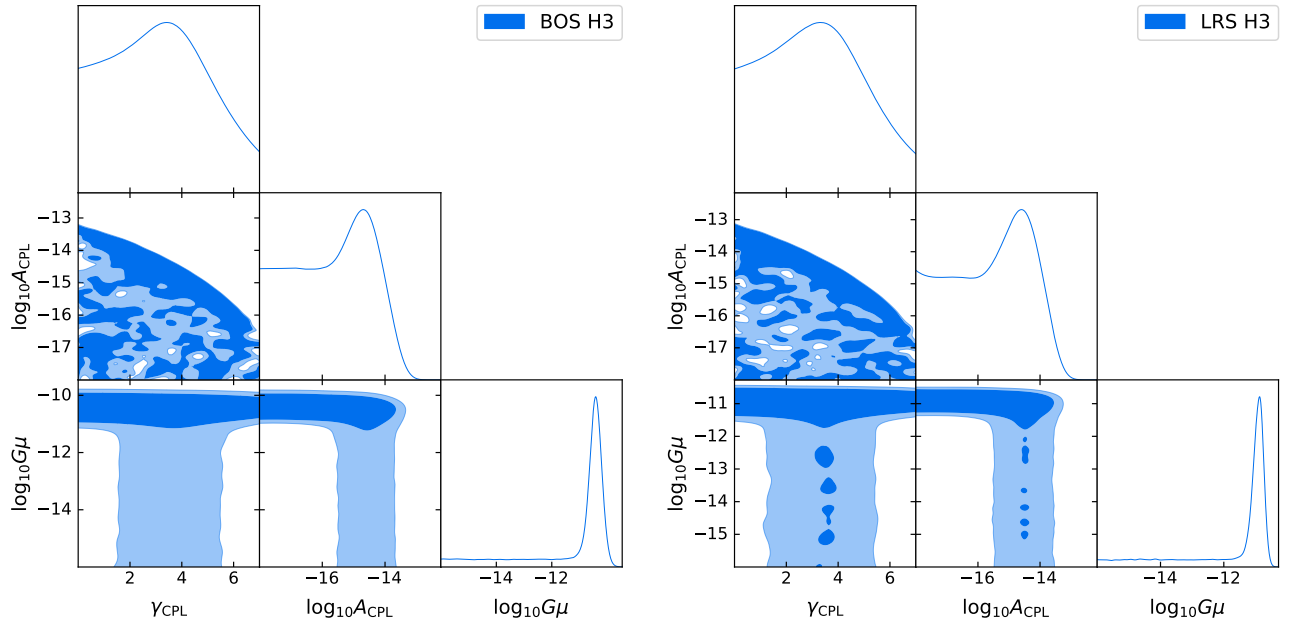


FIG. S3: Posterior distributions of $\log_{10} G\mu$ and the CPL parameters for hypothesis H3, for the BOS (left) and LRS (right) models.

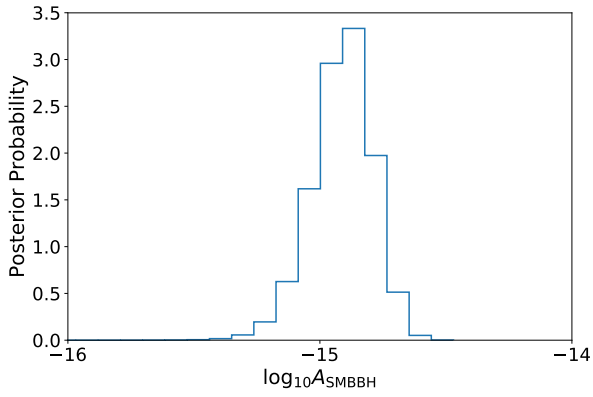


FIG. S4: Posterior distribution of $\log_{10} A_{\text{SMBBH}}$ for the SMBBH-only hypothesis.

treated as a background but with slight changes of the 95% C.L. upper limits of $\log_{10} G\mu$.

TABLE S2: Hypotheses, Bayes factors, and estimated model parameters of different model assumptions for the case with the CPL substituted by the SMBBH.

Hypothesis	Pulsar Noise	SMBBH process	HD process CS spectrum	Bayes Factors	Parameter Estimation (1σ interval)	
					$\log_{10} G\mu$	$\log_{10} A_{\text{SMBBH}}$
H5:SMBBH	✓	✓		$10^{3.3}$ (/H0)		$-14.89^{+0.10}_{-0.12}$
H6:CS3	✓	✓	✓(full hd)	1.21 (/H5)	< -10.05 (95% C.L.)	$-15.11^{+0.25}_{-1.88}$
H7:CS4	✓	✓	✓(full hd)	1.07 (/H5)	< -10.66 (95% C.L.)	$-15.09^{+0.24}_{-1.87}$

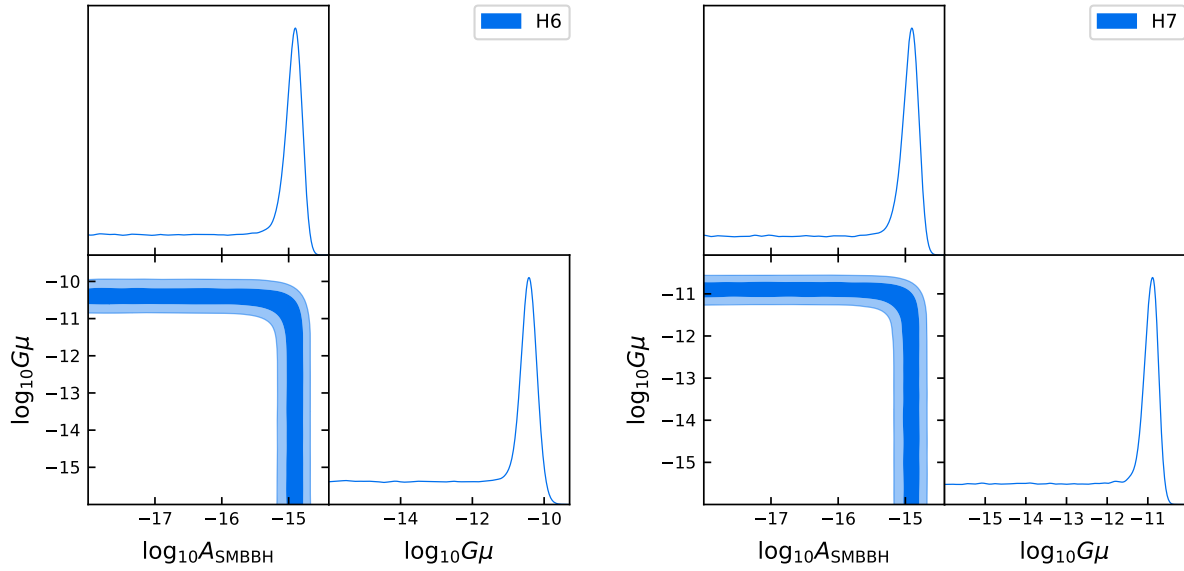


FIG. S5: Posterior distributions of $\log_{10} G\mu$ and $\log_{10} A_{\text{SMBBH}}$ for the BOS (left) and LRS (right) model.